Transition metal redox and Mn disproportional reaction in LiMn0.5Fe0.5PO4 electrodes cycled with aqueous electrolyte

Zengqing Zhuo, Jiangtao Hu, Yandong Duan, Wanli Yang, and Feng Pan

Citation: Applied Physics Letters **109**, 023901 (2016); doi: 10.1063/1.4958639
View online: http://dx.doi.org/10.1063/1.4958639
View Table of Contents: http://scitation.aip.org/content/aip/journal/apl/109/2?ver=pdfcov
Published by the AIP Publishing

Transition metal redox and Mn disproportional reaction in $LiMn_{0.5}Fe_{0.5}PO_4$ electrodes cycled with aqueous electrolyte

Zengqing Zhuo,[1,2,a)] Jiangtao Hu,[1,a)] Yandong Duan,[1,b)] Wanli Yang,[2,b)] and Feng Pan[1,b)]
[1]*School of Advanced Materials, Peking University, Shenzhen Graduate School, Shenzhen 518055, People's Republic of China*
[2]*Advanced Light Source, Lawrence Berkeley National Laboratory, 1 Cyclotron Road, Berkeley, California 94720, USA*

(Received 8 June 2016; accepted 28 June 2016; published online 11 July 2016)

We performed soft x-ray absorption spectroscopy (sXAS) and a quantitative analysis of the transition metal redox in the $LiMn_{0.5}Fe_{0.5}PO_4$ electrodes upon electrochemical cycling. In order to circumvent the complication of the surface reactions with organic electrolyte at high potential, the $LiMn_{0.5}Fe_{0.5}PO_4$ electrodes are cycled with aqueous electrolyte. The analysis of the transitional metal *L*-edge spectra allows a quantitative determination of the redox evolution of Mn and Fe during the electrochemical cycling. The sXAS analysis reveals the evolving Mn oxidation states in $LiMn_{0.5}Fe_{0.5}PO_4$. We found that electrochemically inactive Mn^{2+} is formed on the electrode surface during cycling. Additionally, the signal indicates about 20% concentration of Mn^{4+} at the charged state, providing a strong experimental evidence of the disproportional reaction of Mn^{3+} to Mn^{2+} and Mn^{4+} on the surface of the charged $LiMn_{0.5}Fe_{0.5}PO_4$ electrodes. *Published by AIP Publishing.* [http://dx.doi.org/10.1063/1.4958639]

Lithium ion batteries (LIBs) have played a critical role in our modern society for powering portable electronic devices, electric vehicles, and potentially for the grid-scale storage of renewable energy sources.[1] Significant challenges remain for the development of cathode materials of LIBs that could offer the required long-term stability, safety, and low-cost for the next-generation energy storage. The $LiFePO_4$ based battery electrodes are developed and commercialized with its benefits of low-cost, high thermal stability, and environmental benignity.[2] Recently, attempts to improve the limited energy density of the pristine $LiFePO_4$ lead to the interests in other olivine phosphate compounds, such as $LiMPO_4$ and their solid solutions $LiM_1M_2PO_4$ (M, M_1, and M_2 are transition-metals (TMs), such as Fe, Mn, Co, and Ni). $LiMn_yFe_{1-y}PO_4$, which was first reported by Padhi *et al.*,[2] is one of the most promising candidates to replace their Fe parent compound. The M-O-P inductive effect[3] allows the electrochemical operation at very high potentials, such as Mn^{2+}/Mn^{3+} 4.1 V vs. Li^+/Li.[4]

Extensive studies[4–9] have been performed on $LiMn_yFe_{1-y}PO_4$ electrode materials, and different techniques have been utilized to study the lattice and electronic structures.[5–8,10] Among these extensive studies, soft X-ray absorption spectroscopy (sXAS) provides a direct probe of the transition-metal *3d* states, which allows a quantitative determination of the redox evolution upon electrochemical cycling through the spectral analysis of both the Mn and Fe.[11–14] However, although it is widely believed that both Fe and Mn are involved in the electrochemical cycling, and the cycling potentials of about 3.5 V and 4.1 V stem from the $Fe^{2+/3+}$ and $Mn^{2+/3+}$ redox couples, respectively,[4] the sXAS results reported previously found overwhelming Mn^{2+}, and often shows no change throughout the electrochemical operation of $LiMn_yFe_{1-y}PO_4$ electrodes.[8,15] It is thus proposed that the redox reactions involved in the $LiMn_yFe_{1-y}PO_4$ cycling could be complicated.[7,8,15] While a reliable sXAS analysis is based on the surface sensitive electron yield channel that does not suffer any lineshape distortion,[16] previous measurements have been carried out in non-aqueous electrolyte, which is known to be prone to the surface reactions of the electrodes with organic electrolyte, especially at the high potential. Indeed, it is well known that Mn^{2+} could form on the surface of Mn-based battery compounds especially with the effect of organic electrolyte under high potential.[13,17] Therefore, it is highly desirable to perform sXAS studies of a "clean" system based on aqueous electrolyte, which will circumvent, or partially alleviate, the surface degradation effect for revealing the intrinsic transition metal redox during the cycling of $LiMn_yFe_{1-y}PO_4$ electrodes.

The other issue with $LiMn_yFe_{1-y}PO_4$ electrodes is the nominal Mn^{3+} at the charged state. Mn^{3+} is infamous of the disproportional reaction at the particle surface, i.e., $Mn^{3+} \rightarrow Mn^{2+} + Mn^{4+}$, for example, in spinel $Li_xMn_2O_4$ system.[17] Besides the related structural issues, such reaction generates Mn^{2+}, which leads to the solubility of active cathode materials. Additionally, Mn^{4+} could lead to the instability of the typical organic electrolyte solvents at the electrode-electrolyte interface.[18] Despite of the serious effect of the Mn disproportional reactions on battery performance, there have been no effective technique to probe the reaction experimentally.

In this work, we focus on the quantitative determination of the Mn and Fe redox evolution upon electrochemical cycling of $LiFe_{0.5}Mn_{0.5}PO_4$ electrodes in the aqueous electrolyte system. We show that the quantitative analysis reveals clear experimental evidence on the disproportional

a)Z. Zhuo and J. Hu contributed equally to this work.
b)Authors to whom correspondence should be addressed. Electronic addresses: panfeng@pkusz.edu.cn; wlyang@lbl.gov; and duanyd@pkusz.edu.cn.

reaction of the Mn in $LiFe_{0.5}Mn_{0.5}PO_4$ electrodes at the charged/delithiated state.

We prepared $LiFe_{0.5}Mn_{0.5}PO_4$ nano-crystals as the electrode materials using a reflux method. The preparation and characterization of the $LiFe_{0.5}Mn_{0.5}PO_4$ electrodes is provided in the supplementary material. Both aqueous and non-aqueous systems are tested for the electrochemical profiles. For sXAS and XRD characterizations, electrodes are operated to the desired potentials in a three-electrode aqueous system. The crystallographic structures of the prepared samples are identified by XRD as shown in Fig. 1(a). The diffraction peaks can be perfectly assigned to orthorhombic (Pmnb) Li(Mn, Fe)PO_4.[6] Fig. 1(b) shows the morphology of $LiFe_{0.5}Mn_{0.5}PO_4$ characterized by scanning electron microscopy (SEM), illustrating the mean size of the dispersed material about 40 nm. The elemental composition of the $LiFe_{0.5}Mn_{0.5}PO_4$ is quantitatively determined by inductively coupled plasma atomic emission spectroscopy (ICP-AES), which shows that the ratio of Fe:Mn is 1.0032:1.

Cyclic voltammograms (CV) of $LiFe_{0.5}Mn_{0.5}PO_4$ in aqueous and non-aqueous electrolyte are shown in Figs. 2(a) and 2(b), respectively. In the aqueous system, the saturated calomel electrode (SCE) was used as the reference electrode, and as contrast, in the non-aqueous system, lithium metal was used as the reference. $LiFe_{0.5}Mn_{0.5}PO_4$ exhibits two redox peak in the first cycle with 1 mV s^{-1} in aqueous systems, the anodic and cathodic peaks at 0.27and 0.34 V vs. SCE correspond to 3.51 and 3.58 V vs. Li/Li^+; the anodic and cathodic peak at 0.85 and 0.98 V vs. SCE correspond to 4.09 and 4.22 V vs. Li/Li^+. These potentials are consistent with those in non-aqueous system with a Li/Li^+ reference, which has been attributed to the Fe^{2+}/Fe^{3+} and Mn^{2+}/Mn^{3+} oxidation-reduction reactions.[4] Four samples for sXAS experiments are marked in Fig. 2(c) with different state of charge (SOC), i.e., pristine (P), half charged (1/2Ch), fully charged (Ch), and fully discharged (DisC). The rate capability of $LiFe_{0.5}Mn_{0.5}PO_4$ electrodes are shown in Fig. 2(d), and the mean discharge capacities are 162, 147, 111, 85, and 42 mAh g^{-1} at 0.5, 1, 5, 10, and 50C, respectively. The above electrochemical results show that the $LiFe_{0.5}Mn_{0.5}PO_4$ materials can be electrochemically cycled in aqueous electrolyte with overall similar profile as those in organic electrolyte.

sXAS is performed at Beamline 8.0.1.1 of the Advanced Light Source at Lawrence Berkeley National Laboratory. sXAS is a direct measurement of TM *3d* through dipole-allowed electron excitations. sXAS has advantages over other techniques on probing the key electronic states in the vicinity of the Fermi level, which is relevant to battery performance,[19] such as valence,[11,12] spin states,[14] and local structural effects on the crystal field.[11,14,20] sXAS of Mn and Fe *L*-edge collected through the surface sensitive electron yield mode are conducted on a series of $LiFe_{0.5}Mn_{0.5}PO_4$ electrodes that are electrochemically cycled to the desired SOC in aqueous electrolyte. Here, we focus on the Mn and Fe *L*-edge sXAS lineshape that is sensitive to the different chemical configurations and oxidation states.[11,21]

Fig. 3(a) shows the Fe L_3-edge sXAS results (solid lines) and the fittings (dotted lines) of $LiFe_{0.5}Mn_{0.5}PO_4$ electrodes cycled in aqueous electrolyte to different electrochemical stages. In general, the energy position of main peak shifts from the Fe^{2+} feature at 708.2 eV in sample P to the Fe^{3+} feature at 710.2 eV in samples at half charged state. A quantitative analysis of the evolution of the Fe oxidation states is obtained by fitting the experimental data using a linear combination of two reference spectra, pure Fe^{2+} and Fe^{3+} spectra, shown in supplementary material, Fig. S1.[11] The fitting results (dotted lines in Fig. 3(a)) completely overlap with the experimental data, which validate this method and indicate its high fitting precision. The fitted values of the Fe^{2+} and Fe^{3+} concentrations are plotted in Fig. 3(b). Besides the general $Fe^{2+/3+}$ redox, it is also seen that the re-discharged sample, DisC, displays a combination of 60% Fe^{2+} and 40% Fe^{3+}, which suggests that the Fe redox is not completely reversible in the aqueous electrolyte system. This is consistent with the electrochemical tests that show low capacity retention with extended cycles with aqueous electrolyte. Nonetheless, it is clear that the Fe valence reaches 3+ at the half charged state, which is consistent with the previous report based on organic electrolyte system.[8] Therefore, the analysis shows that the $Fe^{2+/3+}$ redox takes place only at the low potential range of 0.3–0.4 V vs SCE (Fig. 3(b)).

Figs. 4(a) and 4(b) show the Mn *L* absorption features in the two energy regions, L_3 (638–646 eV) and L_2 (649–656 eV), which corresponds to the spin orbit splitting of the *2p* states into $2p^{3/2}$ and $2p^{1/2}$, respectively. The energy position of main peaks in all spectra are located at 639.8 eV, indicating that the existence of Mn^{2+} on the surface throughout the electrochemical operation.[21] The Mn-L sXAS lineshape evolves with electrochemical cycling. The intensity of the Mn^{3+} feature at 641.3 eV becomes stronger with the charge (delithiation) progress,[21] and the lineshape restores

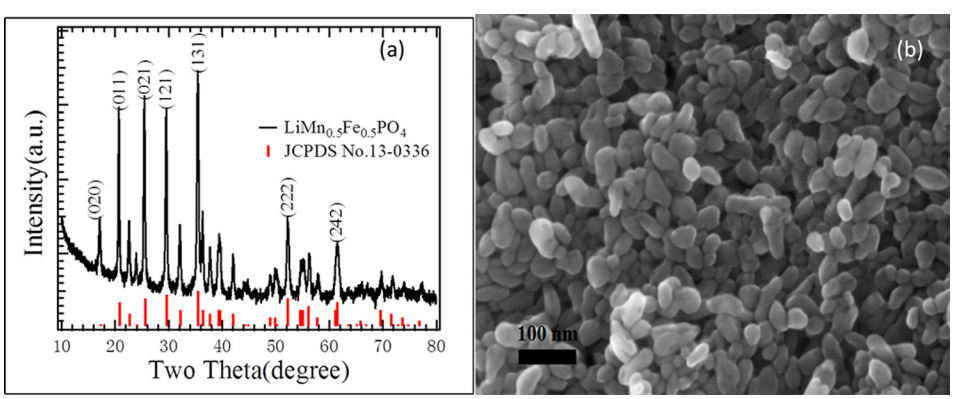

FIG. 1. (a)The powder X-ray diffraction pattern; (b) SEM image of the as-prepared $LiMn_{0.5}Fe_{0.5}PO_4$.

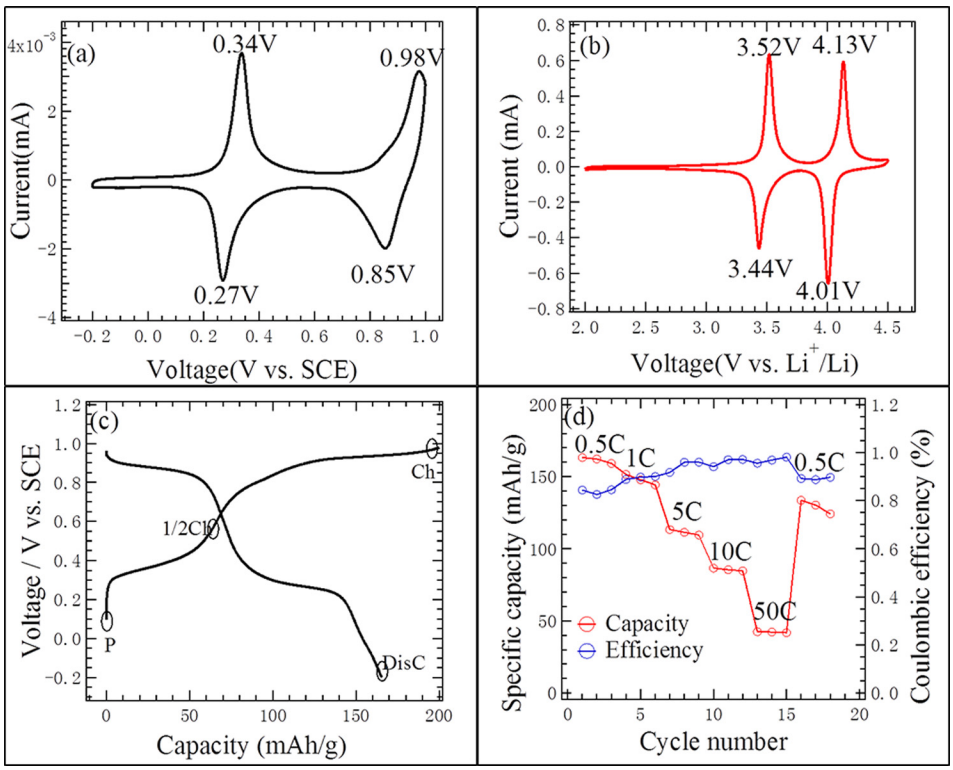

FIG. 2. Cyclic voltammetry profiles of $LiFe_{0.5}Mn_{0.5}PO_4$ run at a scan rate of (a) 1 mV S^{-1} in aqueous electrolyte; (b) 0.2 mV S^{-1} in non-aqueous electrolyte for comparison; (c) the first charge and discharge curves at 0.1C; and (d) the rate performance of $LiMn_{0.5}Fe_{0.5}PO_4$ in aqueous electrolyte.

when fully discharged, revealing that Mn valence changes from Mn^{2+} to Mn^{3+} in the charged samples and changes back to Mn^{2+} in discharged sample. This overall evolution is consistent with the pure $LiMnPO_4$ system.[7] Note that the Mn^{4+} feature around 643.5 eV is also enhanced in the charged samples. This enhancement is consistent with the Mn L_2 features in Fig. 4(b), which displays a shoulder feature of Mn^{4+} at 653.4 eV that is weak but consistently shows up in charged samples. Therefore, although no Mn^{3+}/Mn^{4+} redox is expected by the CV tests, the sXAS data suggest the existence of both Mn^{2+} and Mn^{4+} in the charged (delithiated) states.

Although we are able to observe the Mn redox during the electrochemical cycling with the aqueous electrolyte system, there are two sXAS findings that are inconsistent with the electrochemical profile: the dominating Mn^{2+} feature in all the samples and the weak Mn^{3+} enhancement from half (1/2Ch) to full (Ch) charge where majority of the $Mn^{2+/3+}$ redox reaction supposes to take place.[4] In order to elucidate these discrepancies, we further quantitatively analyse the Mn valence distribution. Fig. 4(c) shows the Mn L_3-edge spectra and the simulations based on a linear combination of the three Mn reference spectra (supplementary material, Fig. S2). Note this method has been demonstrated for studying battery materials.[12,13] The fitting results (dotted lines in Fig. 4(c)) almost completely overlap with the experimental data, validating again this simple method of quantitative analysis.

The calculated concentrations of the Mn^{2+}, Mn^{3+}, and Mn^{4+} are displayed in Fig. 4(d). It can be seen that Mn^{2+} maintains almost 40% concentration, and Mn^{4+} concentration reaches 20% at the fully charged state. Considering the sXAS data through the electron yield channel are collected with a shallow probe depth of only several nanometre on the surface,[22] this result suggests two important properties of the surface of $LiFe_{0.5}Mn_{0.5}PO_4$ electrodes cycled in aqueous electrolyte. First, there is an intrinsic Mn^{2+} layer formation on the surface of the $LiFe_{0.5}Mn_{0.5}PO_4$ electrodes that is electrochemically inactive. Second, the 20% Mn^{4+} concentration strongly indicates the disproportional reaction on the electrode surface, which decreases the contrition of Mn^{3+} while generating Mn^{4+} during the charging process. This effect is strong during the high voltage plateau above 4.1 V after the

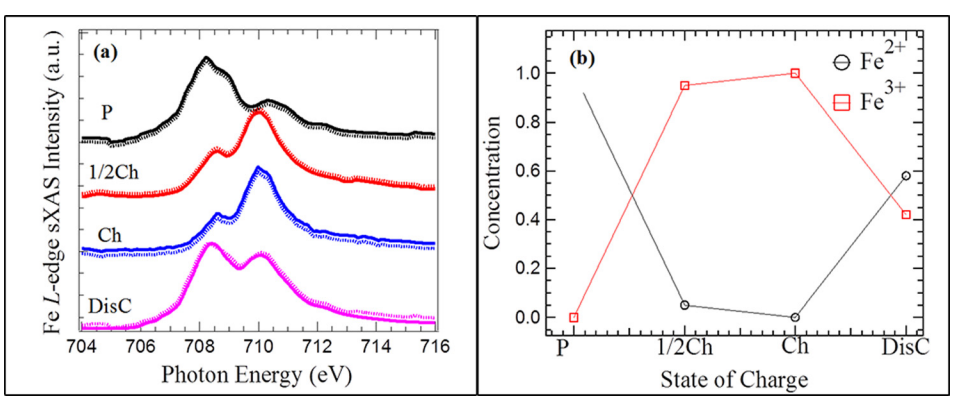

FIG. 3. (a) Fe L-edge spectra (solid line) and quantitative analysis (dotted line) of Fe L-edge spectra; (b) Fe valence evolution of different charge state of $LiMn_{0.5}Fe_{0.5}PO_4$ in aqueous electrolyte.

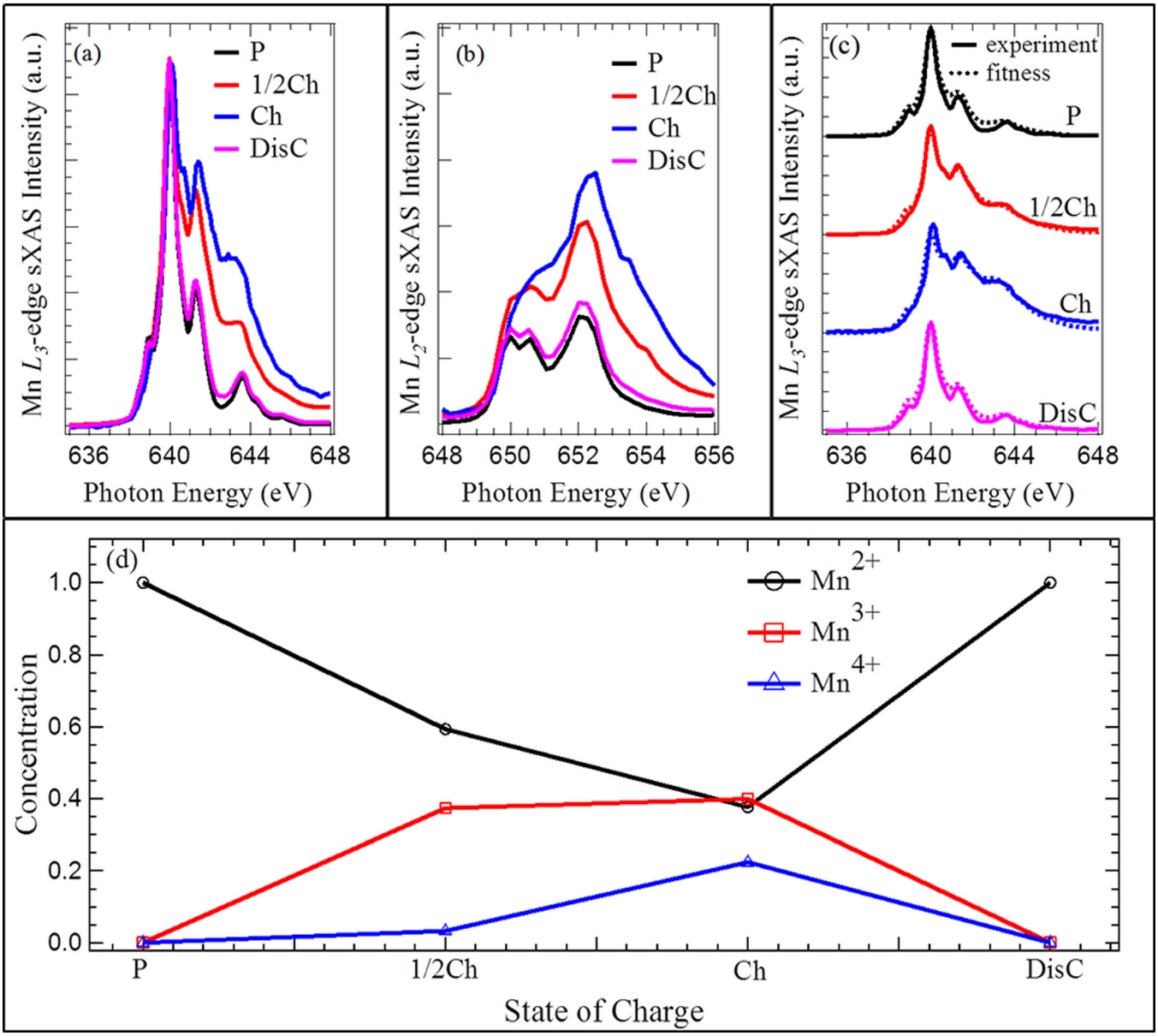

FIG. 4. Mn (a) L_3-edge spectra; (b) L_2-edge spectra of different charge state of $LiFe_{0.5}Mn_{0.5}PO_4$ in aqueous electrolyte; (c) quantitative fitness (dotted line) of Mn L_3-edge spectra; and (d) concentrations of Mn valence at different SOC.

electrode is charged by half. Therefore, our analysis provides a complete understanding of the Mn redox evolution and a strong experimental evidence of the surface disproportional reaction of $Mn^{3+} \rightarrow Mn^{2+} + Mn^{4+}$.

In summary, the $LiMn_{0.5}Fe_{0.5}PO_4$ electrodes with aqueous electrolyte exhibits the Fe and Mn oxidation state evolution in sXAS upon electrochemical cycling, in contrast with the unchanged Mn observed for the cells based on organic electrolyte. Our quantitative analysis of the Fe and Mn redox confirms the $Fe^{2+/3+}$ redox corresponding to the low potential plateau, as expected. More importantly, we found the concentration of about 40% Mn^{2+} and 20% Mn^{4+} on the surface at the charged state. The large amount of Mn^{2+} is likely from the intrinsic material reconstruction on the surface during cycling because we can rule out the interaction effect with organic electrolyte in our aqueous system. The existence of Mn^{4+} provides a strong experimental evidence of the Mn^{3+} disproportional reaction to generate Mn^{2+} and Mn^{4+} on the surface of the $LiMn_{0.5}Fe_{0.5}PO_4$ electrodes. This work demonstrates the employment of aqueous electrolyte and sXAS for probing an electrode surface redox reaction that is free of organic electrolyte effect, which could be extended to other electrode systems for revealing the intrinsic redox evolution during the electrochemical operation.

See supplementary material for a full description of the electrode preparation and electrochemical characterization along with details regarding the XAS.

This work was supported by Guangdong Innovation Team Project (No. 2013N080) and Shenzhen Science and Technology Research Grant (peacock plan KYPT20141016105435850). Advanced Light Source is supported by the Director, Office of Science, Office of Basic Energy Sciences, of the U.S. Department of Energy under Contract No. DE-AC02-05CH11231.

[1]J. B. Goodenough and Y. Kim, Chem. Mater. **22**(3), 587 (2010); P. G. Bruce, Solid State Ionics **179**(21–26), 752 (2008); M. Armand and J. M. Tarascon, Nature **451**(7179), 652 (2008).
[2]A. K. Padhi, K. S. Nanjundaswamy, and J. B. Goodenough, J. Electrochem. Soc. **144**(4), 1188 (1997).
[3]A. K. Padhi, K. S. Nanjundaswamy, C. Masquelier, S. Okada, and J. B. Goodenough, J. Electrochem. Soc. **144**(5), 1609 (1997).
[4]S. K. Martha, J. Grinblat, O. Haik, E. Zinigrad, T. Drezen, J. H. Miners, I. Exnar, A. Kay, B. Markovsky, and D. Aurbach, Angew. Chem., Int. Ed. **48**(45), 8559 (2009).
[5]I. Bezza, M. Kaus, R. Heinzmann, M. Yavuz, M. Knapp, S. Mangold, S. Doyle, C. P. Grey, H. Ehrenberg, S. Indris, and I. Saadoune, J. Phys. Chem. C **119**(17), 9016 (2015).
[6]J. Bai, J. Hong, H. Chen, J. Graetz, and F. Wang, J. Phys. Chem. C **119**(5), 2266 (2015).
[7]L. F. J. Piper, N. F. Quackenbush, S. Sallis, D. O. Scanlon, G. W. Watson, K. W. Nam, X. Q. Yang, K. E. Smith, F. Omenya, N. A. Chernova, and M. S. Whittingham, J. Phys. Chem. C **117**(20), 10383 (2013).
[8]S. Kurosumi, K. Horiba, N. Nagamura, S. Toyoda, H. Kumigashira, M. Oshima, S. Furutsuki, S.-i. Nishimura, A. Yamada, and N. Mizuno, J. Power Sources **226**, 42 (2013).
[9]A. Guéguen, L. Castro, R. Dedryvère, E. Dumont, J. Bréger, C. Tessier, and D. Gonbeau, J. Electrochem. Soc. **160**(2), A387 (2013); H. Wang, Y. Yang, Y. Liang, L. F. Cui, H. S. Casalongue, Y. Li, G. Hong, Y. Cui, and H. Dai, Angew. Chem., Int. Ed. **50**(32), 7364 (2011).
[10]D. B. Ravnsbaek, K. Xiang, W. Xing, O. J. Borkiewicz, K. M. Wiaderek, P. Gionet, K. W. Chapman, P. J. Chupas, and Y. M. Chiang, Nano Lett. **14**(3), 1484 (2014).
[11]X. Liu, J. Liu, R. Qiao, Y. Yu, H. Li, L. Suo, Y.-s. Hu, Y.-D. Chuang, G. Shu, F. Chou, T.-C. Weng, D. Nordlund, D. Sokaras, Y. J. Wang, H. Lin, B. Barbiellini, A. Bansil, X. Song, Z. Liu, S. Yan, G. Liu, S. Qiao, T. J. Richardson, D. Prendergast, Z. Hussain, F. M. F. de Groot, and W. Yang, J. Am. Chem. Soc. **134**(33), 13708 (2012).
[12]R. Qiao, K. Dai, J. Mao, T.-C. Weng, D. Sokaras, D. Nordlund, X. Song, V. S. Battaglia, Z. Hussain, G. Liu, and W. Yang, Nano Energy **16**, 186 (2015).
[13]R. Qiao, Y. Wang, P. Olalde-Velasco, H. Li, Y.-S. Hu, and W. Yang, J. Power Sources **273**, 1120 (2015).
[14]L. Wang, J. Song, R. Qiao, L. A. Wray, M. A. Hossain, Y.-D. Chuang, W. Yang, Y. Lu, D. Evans, J.-J. Lee, S. Vail, X. Zhao, M. Nishijima, S. Kakimoto, and J. B. Goodenough, J. Am. Chem. Soc. **137**(7), 2548 (2015).
[15]H. M. Hollmark, T. Gustafsson, K. Edstrom, and L. C. Duda, Phys. Chem. Chem. Phys. **13**(45), 20215 (2011).
[16]F. d. Groot and A. Kotani, *Core Level Spectroscopy of Solids* (CRC Press Taylor & Francis Group, Boca Raton, London, New York, 2008).
[17]M. M. Thackeray, Y. Shao-Horn, A. J. Kahaian, K. D. Kepler, E. Skinner, J. T. Vaughey, and S. A. Hackney, Electrochem. Solid-State Lett. **1**(1), 7 (1998).
[18]Y. Su, S. Cui, Z. Zhuo, W. Yang, X. Wang, and F. Pan, ACS Appl. Mater. Interfaces **7**(45), 25105 (2015).
[19]W. Yang, X. Liu, R. Qiao, P. Olalde-Velasco, J. D. Spear, L. Roseguo, J. X. Pepper, Y.-d. Chuang, J. D. Denlinger, and Z. Hussain, J. Electron Spectrosc. Relat. Phenom. **190**, 64 (2013); Y. Wanli and Q. Ruimin, Chin. Phys. B **25**(1), 017104 (2016).
[20]X. Liu, Y. J. Wang, B. Barbiellini, H. Hafiz, S. Basak, J. Liu, T. Richardson, G. Shu, F. Chou, T.-C. Weng, D. Nordlund, D. Sokaras, B. Moritz, T. P. Devereaux, R. Qiao, Y.-D. Chuang, A. Bansil, Z. Hussain, and W. Yang, Phys. Chem. Chem. Phys. **17**(39), 26369 (2015).
[21]R. Qiao, T. Chin, S. J. Harris, S. Yan, and W. Yang, Curr. Appl. Phys. **13**(3), 544 (2013).
[22]R. Qiao, I. T. Lucas, A. Karim, J. Syzdek, X. Liu, W. Chen, K. Persson, R. Kostecki, and W. Yang, Adv. Mater. Interfaces **1**(3), 1300115 (2014).